

Retained Myogenic Potency of Human Satellite Cells from Torn Rotator Cuff Muscles Despite Fatty Infiltration

Masashi Koide,¹ Yoshihiro Hagiwara,¹ Masahiro Tsuchiya,² Makoto Kanzaki,³ Hiroyasu Hatakeyama,^{3,4} Yukinori Tanaka,⁵ Takashi Minowa,⁶ Taro Takemura,⁶ Akira Ando,¹ Takuya Sekiguchi,¹ Yutaka Yabe¹ and Eiji Itoi¹

¹Department of Orthopaedic Surgery, Tohoku University Graduate School of Medicine, Sendai, Miyagi, Japan

²Tohoku Fukushi University, Sendai, Miyagi, Japan

³Graduate School of Biomedical Engineering, Tohoku University, Sendai, Miyagi, Japan

⁴Frontier Research Institute for Interdisciplinary Sciences, Tohoku University, Sendai, Miyagi, Japan

⁵Department of Oral Immunology, Tohoku University Graduate School of Dentistry, Sendai, Miyagi, Japan

⁶National Institute for Materials Science, Tsukuba, Ibaraki, Japan

Rotator cuff tears (RCTs) are a common shoulder problem in the elderly that can lead to both muscle atrophy and fatty infiltration due to less physical load. Satellite cells, quiescent cells under the basal lamina of skeletal muscle fibers, play a major role in muscle regeneration. However, the myogenic potency of human satellite cells in muscles with fatty infiltration is unclear due to the difficulty in isolating from small samples, and the mechanism of the progression of fatty infiltration has not been elucidated. The purpose of this study was to analyze the population of myogenic and adipogenic cells in disused supraspinatus (SSP) and intact subscapularis (SSC) muscles of the RCTs from the same patients using fluorescence-activated cell sorting. The microstructure of the muscle with fatty infiltration was observed as a whole mount condition under multi-photon microscopy. Myogenic differentiation potential and gene expression were evaluated in satellite cells. The results showed that the SSP muscle with greater fatty infiltration surrounded by collagen fibers compared with the SSC muscle under multi-photon microscopy. A positive correlation was observed between the ratio of muscle volume to fat volume and the ratio of myogenic precursor to adipogenic precursor. Although no difference was observed in the myogenic potential between the two groups in cell culture, satellite cells in the disused SSP muscle showed higher intrinsic myogenic gene expression than those in the intact SSC muscle. Our results indicate that satellite cells from the disused SSP retain sufficient potential of muscle growth despite the fatty infiltration.

Keywords: arthroscopic surgery; fatty infiltration; muscle; rotator cuff tear; satellite cell

Tohoku J. Exp. Med., 2018 January, 244 (1), 15-24. © 2018 Tohoku University Medical Press

Introduction

Rotator cuff tears (RCTs) are a common shoulder problem in the elderly that can obstruct the performance of routine activities (Gladstone et al. 2007; Barry et al. 2013). Approximately 30% of individuals > 60 years old have a full-thickness RCT (Tempelhof et al. 1999). The surgical outcome in patients with large or massive tears is generally unsatisfactory due to the poor condition of tendons or affected muscles (Gladstone et al. 2007; Fermont et al. 2014). Severely damaged RCTs induce muscle atrophy with fatty infiltration (Oh et al. 2014), which does not improve with surgery (Gladstone et al. 2007) and is a prognostic factor for post-surgical outcomes (Fermont et al. 2014).

Muscle satellite cells have been considered to be

reduced after disuse by impaired proliferation (Li et al. 2016). Muscle satellite cells are typical muscle stem cells that exhibit self-renewal and myogenic differentiation capacities (Judson et al. 2013; Gigliotti et al. 2016) and are characterized by expression of cluster of differentiation 56 (CD56) in humans (Boldrin et al. 2010). These generally quiescent cells are located between the basal lamina and sarcolemma of the skeletal muscle fibers (Zammit et al. 2006). The physical load of muscles rapidly induces satellite cell activation and proliferation for damage repair and muscle regeneration (Zammit et al. 2006). It remains unclear whether human satellite cells maintain muscle regeneration capacity in disused muscles, regardless of RCT severity (Meyer et al. 2015).

Fatty infiltration into skeletal muscles is thought to cause muscle degeneration by impairing the myogenic

Received July 24, 2017; revised and accepted December 11, 2017. Published online December 28, 2017; doi: 10.1620/tjem.244.15.

Correspondence: Yoshihiro Hagiwara, Department of Orthopaedic Surgery, Tohoku University Graduate School of Medicine, 1-1 Seiryomachi, Aoba-ku, Sendai, Miyagi 980-8574, Japan.
e-mail: hagi@med.tohoku.ac.jp

function of satellite cells (Pisani et al. 2010), although the underlying mechanism is not well understood. However, it has pathological similarities to muscular diseases, such as sarcopenia and muscular dystrophies (Uezumi et al. 2010). Adipocytes originate from mesenchymal stem cells that reside in the interstitial regions of human skeletal muscles and are characterized by CD45/CD31 negativity and expression of platelet-derived growth factor receptor alpha (PDGFR α) (Uezumi et al. 2014). PDGFR α -positive cells are a major source of adipocytes in disused murine muscles with fatty infiltration (Liu et al. 2016; Davies et al. 2016). However, how pathophysiological conditions influence adipogenic precursors in human skeletal muscles is unclear (Pisani et al. 2010; Perruchot et al. 2013).

To this end, the present study compared torn disused supraspinatus (SSP) and intact subscapularis (SSC) muscle satellite cells and adipogenic precursor populations in the RCTs. Muscle atrophy of disused muscle was evaluated using magnetic resonance imaging (MRI), and the satellite cell potential to differentiate into myotubes was examined. Furthermore, we examined the gene expression patterns between SSC and SSP cells to clarify whether less physical load affects the myogenic potentials of satellite cells.

Patients and Methods

Study population and sample collection

The study protocol was approved by the Tohoku University Hospital's Institutional Review Board (approval number: 2014-1-703), and written informed consent was obtained from all participants. From January 2015 to December 2015, we performed arthroscopic RCT repair in 42 patients who were unresponsive to conservative treatments. Muscle samples were collected from 19 patients who agreed to undergo biopsy. Four patients were excluded in the data analysis because of technical problems. The number of patients evaluated was restricted because of limited access to the fluorescence-activated cell sorting (FACS) system at our institute and the requirement for performing the procedure on the same day as the surgery. The cells prepared from each muscle by FACS were separated into three replicates for characterization and culture. None of the patients had tears in the SSC tendon based on both magnetic resonance imaging (MRI) and arthroscopic findings. Fatty infiltration of the rotator cuff muscle was identified using MRI and classified into the following five stages based on the modified Goutallier classification (Goutallier et al. 1994; Fuchs et al. 1999): 0, normal; 1, some fat streaks; 2, fatty degeneration of < 50%; 3, 50% fatty muscle atrophy; and 4, fatty infiltration of > 50%. Satellite cells from both SSC and SSP muscles were compared in the same patient. None of the patients had muscular disease, neurovascular problems, paralysis, or trauma. Muscle biopsy specimens (approximately 300 mg) were obtained from the same portion of the muscle belly of the SSP and SSC muscles in each patient who underwent arthroscopic surgery. The SSC muscle specimen was obtained from the back side after a release of the joint capsule, and the SSP muscle specimen was obtained from the bursal side around the scapular spine after release of the synovial bursa. The mean age of the patients was 65.4 ± 8.44 years (47-76 years; 9 men and 6 women) (Table 1).

Multi-photon microscopy

The micro-structure of the SSP and SSC muscle tissue samples was evaluated using multi-photon three-dimensional imaging. The samples were collected and immediately fixed overnight with 4% paraformaldehyde in 0.1-M phosphate buffer (pH 7.4) containing 18% sucrose. The sample was washed thrice with phosphate-buffered saline (PBS) and stained for 30 min at 4°C with BODIPY 558/568 C12 (final concentration: 5 μ M; Life Technologies, Carlsbad, CA, USA) for adipose tissue staining, Hoechst 33342 (final concentration: 40 μ M; Dojindo Molecular Technologies, Kumamoto, Japan) for nuclear staining, and Alexa Fluor 488-conjugated isolectin GS-IB4 (final concentration: 10 μ g/ml, Life Technologies) for endothelial cell staining. The signal of the collagenous fibers can be detected as second harmonic generation (SHG) without staining. The photographs of the samples were obtained using a multi-photon imaging system, consisting of an upright microscope (A1R-MP+; Nikon, Tokyo, Japan) equipped with a Ti-sapphire laser (Mai-Tai DeepSee; Spectra-Physics, Santa Clara, CA) and a 25 \times water objective lens (N.A. = 1.10). The samples were excited at 920 nm, and signals were detected using GaAsP-type non-descanned detectors at 425-475 nm for SHG signals and Hoechst 33342 (blue channel), at 500-550 nm for Alexa Fluor 488 (green channel), and at 601-657 nm for BODIPY 558/568 (red channel). Image stacks consisting of 280 optical sections with 2- μ m z-steps were acquired, and 3D reconstruction was performed with NIS Element software (Nikon).

Cell isolation and proliferation

The tissue samples were washed with normal saline to remove blood cells and transferred to sterile Dulbecco's Modified Eagle's Medium (DMEM; Wako Pure Chemicals Industries, Osaka, Japan) supplemented with 1% penicillin-streptomycin. The tissue was minced and digested with 0.2% collagenase (Wako Pure Chemicals Industries) and 0.1% DNase I (Sigma-Aldrich, St. Louis, MO, USA) for 1 h at 37°C. PBS was added to digested muscle tissue samples, which were filtered through a 70- μ m cell strainer (BD Biosciences, Franklin Lakes, NJ, USA) and centrifuged at 700 g for 20 min. Pellets were resuspended in 1-ml staining solution composed of 1% bovine serum albumin (BSA; Sigma-Aldrich) in PBS and then incubated with an Fc receptor blocking solution (Human TruStain FcX, 1:20 in staining buffer; Biolegend, San Diego, CA, USA) for 10 min. The samples were then labeled with the following monoclonal antibodies (all from Biolegend and all at 1:20 dilution): fluorescein isothiocyanate (FITC)-conjugated anti-CD45 (clone HI30), FITC-conjugated anti-CD11b (clone ICRF444), FITC-conjugated anti-CD31 (clone WM59), phycoerythrin (PE)/Cy7-conjugated anti-CD34 (clone 581), allophycocyanin (APC)-conjugated anti-CD56 (clone MEM-188), and PE-conjugated anti-PDGFR α (clone 16A1). The negative set included blood markers CD11b and CD45, and endothelial markers CD31 and CD34. CD34 is known to be expressed by the majority of mouse satellite cells (Bareja et al. 2014). In contrast, human muscle-derived CD34⁺ cells are myogenic and adipogenic, whereas CD34⁻ cells are myogenic and not adipogenic (Pisani et al. 2010). Therefore, CD34 was used as a negative selection marker in this study. After 45-min incubation on ice, the cell suspension was washed with staining solution and centrifuged twice for 5 min at 700 g. Human satellite cells were defined as single live mononuclear CD11b⁻CD31⁻CD34⁻CD45⁺CD56⁺ cells, and adipogenic precursors were defined as CD11b⁻CD31⁻CD45⁺PDGFR α ⁺ cells (Uezumi et al. 2014; Bareja et al. 2014). FACS was performed on a FACS ARIA II

Table 1. Recruited patients' ID, FACS, and MRI.

ID	Year	Sex		CD56 cell	PDGFR α cell	CD56/PDGFR α	MRI (Muscle atrophy)
1	71	F	SSC	0.0537	0.0072	7.4767	0.6622
			SSP	0.0075	0.0050	1.5192	0.1979
2	47	M	SSC	0.0420	0.0053	8.0000	0.8845
			SSP	0.0347	0.0086	4.0231	0.3447
3	66	M	SSC	0.0762	0.0056	13.6752	0.9199
			SSP	0.0511	0.0121	4.2218	0.3320
4	69	M	SSC	0.4769	0.0515	9.2602	0.8755
			SSP	0.1419	0.0487	2.9138	0.4362
5	48	M	SSC	0.4279	0.1448	2.9551	0.6485
			SSP	0.4328	0.1026	4.2191	0.6593
6	66	F	SSC	0.0827	0.0720	1.1481	0.4013
			SSP	0.1043	0.1782	0.5852	0.1993
7	67	M	SSC	0.1598	0.0598	2.6745	0.4176
			SSP	0.0569	0.1775	0.3204	0.0953
8	69	M	SSC	0.0541	0.0093	5.7941	0.9039
			SSP	0.0480	0.0389	1.2326	0.4985
9	74	M	SSC	0.2935	0.0606	4.8434	0.8615
			SSP	0.3006	0.1113	2.7010	0.2632
10	71	F	SSC	0.0482	0.0091	5.2790	0.7019
			SSP	0.0732	0.0228	3.2152	0.2991
11	69	F	SSC	0.0944	0.0082	11.5802	0.8561
			SSP	0.0791	0.0364	2.1748	0.1713
12	60	F	SSC	0.1019	0.0135	7.5337	0.8059
			SSP	0.2767	0.0490	5.6456	0.3677
13	68	M	SSC	0.2918	0.0351	8.3085	0.6679
			SSP	0.2252	0.0972	2.3176	0.1901
14	60	M	SSC	0.0772	0.0439	1.7577	0.7312
			SSP	0.1289	0.5074	0.2540	0.3632
15	76	F	SSC	0.4581	0.5110	0.8965	0.7584
			SSP	0.0298	0.0618	0.4816	0.2929

Total 15 patients were analyzed by FACS and MRI. The mean age of the patients was 65.4 ± 8.44 years (47-76 years; 9 men and 6 women). The ratios of CD56 cell and PDGFR α cell population to total particle, and the ratio of CD56 cell to PDGFR α cell population are presented. The muscle atrophy was determined by using the scapular Y view of MRI. The area of the SSP and SSC muscle belly to the area of each muscle's fossa of the scapula was calculated as muscle atrophy.

flow cytometer (BD Biosciences), and data were analyzed with the FlowJo software (Tree Star, Ashland, OR, USA). The sorting gate was set by the negative control treated with Fc receptor blocking solution. Cells were seeded on 24-well chamber slides coated with Matrigel (Dow Corning, Corning, NY, USA) in a growth medium containing DMEM/Ham's F10 mixture supplemented with 20% fetal bovine serum, 1% penicillin-streptomycin, 10% chicken embryonic extract (United States Biological, Salem, MA, USA), and 2.5-ng/ml basic fibroblast growth factor (Thermo Fischer Scientific, Waltham, MA, USA) and incubated at 37°C under 5% CO₂ atmosphere. When cells reached 80%-90% of confluence, adherent cells were dissociated by treatment with 1 mM EDTA and passaged to a new Matrigel-coated 10-cm dish. Because adipogenic precursors showed insufficient proliferation, only satellite cells were stored in liquid nitrogen.

Immunofluorescence analysis

Satellite cells were seeded in Matrigel-coated 6-well plates. To ensure satellite cell purity, CD11b⁻CD31⁻CD34⁻CD45⁻CD56⁺ cells isolated by FACS were labeled with antibodies against PAX7 (ab34360; Abcam, Cambridge, UK) or MyoD (M-318; Santa Cruz Biotechnology, Dallas, TX, USA). The most reliable markers of

human satellite cells are PAX7 and CD56 (Boldrin et al. 2010), and MyoD expression in satellite cells has been previously reported to depend on myogenic differentiation (Bareja et al. 2014). Myogenic differentiation was induced by replacing the growth medium with DMEM/Ham's F10 mixture supplemented with 5% horse serum and 1% penicillin-streptomycin (Asakura et al. 2002). The differentiation medium was changed every 24 h. For immunofluorescence labeling, cells were grown on Matrigel-coated 22-mm glass coverslips (C022221; Matsunami, Osaka, Japan) in 6-well plates. After experimental treatments, cells were washed with PBS and fixed for 20 min with 2% paraformaldehyde in PBS containing 0.1% Triton X-100, then washed and blocked in PBS containing 5% calf serum with 1% BSA for 1 h at room temperature. Anti-human myosin heavy chain antibody (MAB4470; R&D Systems, Minneapolis, MN, USA) and Alexa Fluor 594-conjugated anti-mouse IgG secondary antibody (Thermo Fischer Scientific) were used at 1:100 and 1:1,000 dilutions, respectively, in a solution of 1% BSA in PBS. The samples were mounted on glass slides with Vectashield (Vector Laboratories, Burlingame, CA, USA) and observed with a confocal fluorescence microscope (Fluoview FV-1000; Olympus, Tokyo, Japan) and ASW v.1.3 software (Olympus). Images were imported into Adobe

Photoshop 6.0 (Adobe Systems, San Jose, CA, USA) and Image-Pro Plus (Media Cybernetics, Rockville, MD, USA) for processing. Myotubes, defined as positive for myosin heavy chain and harboring nuclei, were counted within a $500 \times 500\text{-}\mu\text{m}$ area as the number of DAPI-stained nuclei inside the cell. The fusion rate was classified into three groups based on the number of nuclei in myotubes (1 to 3, 4 to 10, and > 10). At least five random microscopic fields were counted for each sample under $200 \times$ magnification, and at least three independent experiments were performed for each condition (Ariga et al. 2008).

MRI quantification

Muscle/adipose tissue ratios of SSP and SSC muscles were evaluated using MRI (Hitachi Medical Corporation, Tokyo, Japan) before arthroscopic surgery. The muscle atrophy ratio was determined based on the Goutallier protocol (Goutallier et al. 1994) by analyzing the most lateral sagittal-oblique image where the acromion, coracoid, and scapular body were all visible, along with the next two consecutive lateral images (Barry et al. 2013). Using the scapular Y view of MRI, the area of the SSP and SSC muscle belly to the area of each muscle's fossa of the scapula was calculated as muscle atrophy.

DNA microarray

Two pairs of satellite cells derived from muscle samples (Patients 1 and 7; Table 1) were used for DNA microarray analysis. Two particular samples were chosen for the microarray analysis because they were from the first series of samples that could be used for the microarray study in both the SSC and SSP groups. No clinical data were collected, except age, sex, and the fatty infiltration seen on MRI, in this study. After treatment with DNase I (Invitrogen, Carlsbad, CA, USA), RNA was amplified using the Amino Allyl MessageAmp II aRNA Amplification kit (Ambion, Austin, TX, USA) and labeled with Cy3 and Cy5, then hybridized to a whole Human Genome Microarray 4×44 K (Agilent Technologies, Santa Clara, CA, USA) at 65°C for 17 h (Yamayoshi et al. 2012). The array was scanned with GenePix 4000B (Molecular Devices, Downingtown, PA, USA), and the scanned image was analyzed with GenePix Pro 6

software (Molecular Devices) (Hagiwara et al. 2012). To obtain gene expression profiles, probes for which the average expression level was upregulated (> 3.0 times) or downregulated ($< 1/3$ times) in satellite cells from the SSP muscle were compared with those from the SSC muscle (Hagiwara et al. 2012; Yabe et al. 2015).

Quantitative real-time polymerase chain reaction (qRT-PCR)

After experimental treatment and switching of culture medium, total RNA was extracted from satellite cells with TRIzol reagent (Invitrogen) and reverse transcribed using the Transcriptor First Strand cDNA Synthesis kit (Roche Diagnostics, Minneapolis, MN, USA) with oligo-dT primer. The cDNA was used for qRT-PCR on a CFX96 system (Bio-Rad, Hercules, CA, USA). The relative expression levels of target genes were determined using the $2^{-\Delta\Delta\text{CT}}$ method (Pfaffl 2001). PCR efficiency and expression levels of myogenic differentiation factors relative to elongation factor $1\alpha 1$ were calculated as previously described (Yabe et al. 2015). Primer sequences are listed in Table 2.

Statistical analysis

Data were analyzed with SPSS v.23.0 (SPSS Japan, Tokyo, Japan). Experimental values were presented as mean \pm standard error of the mean. Because the data in this study were considered non-parametric, the mean differences were evaluated using the Mann-Whitney U test. P values < 0.05 were considered statistically significant.

Results

Proportion of myogenic/adipogenic precursors

Satellite cells constituted 0.17% (± 0.036) and 0.12% (± 0.027) of the total particles in the SSC and SSP muscles, respectively (15 specimens for each group) (Fig. 1A-F). No significant differences were observed in the satellite cell population between the two groups (Fig. 1G). More adipogenic precursors were found in the SSP muscle than in the SSC muscle ($0.077 \pm 0.030\%$ and $0.110 \pm 0.028\%$, respec-

Table 2. Primer sequences for qRT-PCR.

Primer	Forward	Reverse
MYL1	TTAAGCCAGGTCGGTGATGTCC	GGTGGCCTGGTCCTTGTGTGT
KCNA1	GGTGGGCGGTGGTGTC	CCCCTCAGTTTCTCGGTGGTAG
HOXA11	CGCCTCCTCCGACTACCC	CCGCCGCTCTTTCTCCTC
MYH2	GGACCCCCTGAATGAGACC	CAGCAGTTTGAGCCCCAGAG
MMP3	GATGCCCACTTTGATGATGATGAA	AGTGTTGGCTGAGTGAAAGAGACC
SEPP1	TCGGGCAGAGGAGAACATAA	AGCGTCAACTGGCACTGG
PCSK1	GACTTGCGGAATCACTCTGT	TTTCCGGGCCAATCTAAG
CCDC3	CGGGAGCGAGTGAAGAAGGTC	CCCCGGGCGTTGATGTG
HOX C4	GGCGCTCCCTTCATTAG	CCCCAGCTTCGGCAACT
HOX C6	AACCGCCGGATGAAGTGGA	AGAGGGGTGGCAGGGACT
SIM2	GGCGGTGGGTGGCAGAT	CCCCGAGGCAGGCAGAC
HOXA11-AS	ATGGCCATGAAGGGGAAGAACT	GAGGCGCTGGGCAACTGTC
F2RL2	GCCGGGCCACCACAGTC	GTTGCCACACCAGTCCACAT

The gene expression of satellite cells in SSC and SSP muscle of MYL1, KCNA1, HOXA11, MYH2, MMP3, SEPP1, PCSK1, CCDC3, HOX C4, HOX C6, SIM2, HOXA11-AS, and F2RL2 were analyzed by qRT-PCR.

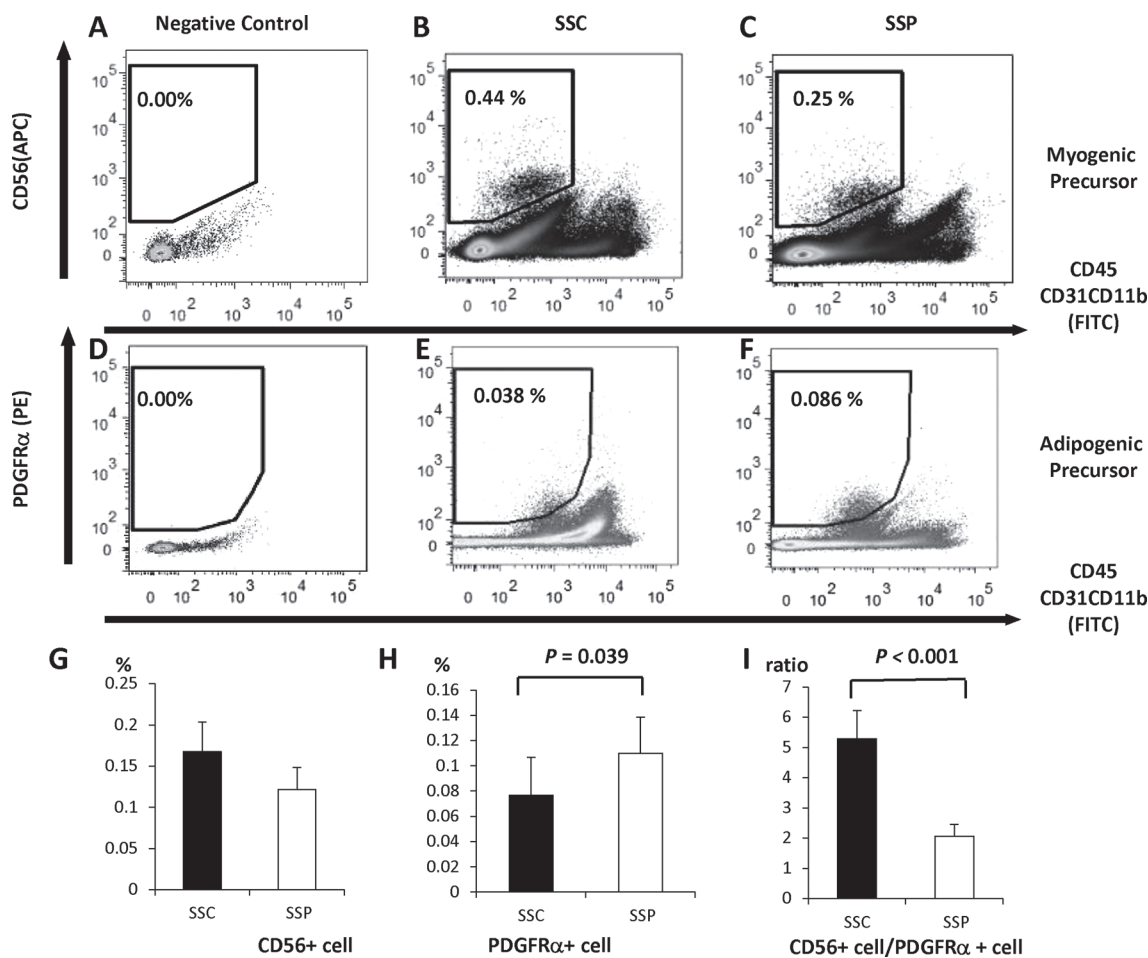


Fig. 1. Flow cytometry analysis of rotator cuff muscles.

A-F: Scatterplots for negative control (A and D), SSC muscle (B and E), and SSP muscle (C and F). The representative data are presented, and the similar results were obtained with other muscle specimens ($n = 15$ for each group). G: Population ratio of myogenic precursors to total particles. H: Population ratio of adipogenic precursors to total particles. I: Ratio of myogenic precursors to adipogenic precursors. Satellite cells (B and C) and adipogenic precursors (E and F) of SSC and SSP muscles were analyzed using fluorescence-activated cell sorting (FACS). The sorting gate is set by the negative control treated with Fc receptor-blocking solution (A and D). No differences are observed in satellite cell populations between the two groups ($P = 0.17$) (G), whereas adipogenic precursor ratios in the SSP muscle are higher than those in the SSC muscle ($P = 0.039$) (H). Satellite cell/adipogenic precursor ratio in the SSC muscle is higher than that in the SSP muscle ($P < 0.001$) (I). Data represent mean \pm standard error of the mean.

tively; $P = 0.039$) (Fig. 1H). The ratio of satellite cells to adipogenic precursors was lower in the SSP muscle than in the SSC muscle ($P < 0.001$) (Fig. 1I).

The ratio of myogenic precursor to adipogenic precursor was used as an indicator of muscle atrophy. A positive correlation ($R^2 = 0.5459$, $P < 0.001$) was found between the muscle atrophy ratio evaluated by MRI and the precursor ratio (Fig. 2). Because of the fatty infiltration on MRI, we analyzed the intra-muscular adipose tissues in the SSP muscle using multi-photon microscopy imaging (Fig. 3), showing the greater fatty infiltration in the SSP muscle, compared with the SSC muscle.

Myogenic potential of satellite cells derived from atrophic muscles

The purity of the sorted satellite cells was confirmed by immunostaining with PAX7 (Fig. 4A-C) and MyoD (Fig.

4D-F). Most cells showed PAX7 positivity (Fig. 4G), whereas approximately 20% cells were labeled with anti-MyoD antibody (Fig. 4H). No statistically significant difference was found between the SSP and SSC groups in the ratio of MyoD-positive cell to total PAX7-positive cell. Satellite cells in SSC and SSP muscles were differentiated into myoblasts and myotubes that were identified based on myosin heavy chain (MHC) immunoreactivity (Fig. 5A). The number of multi-nucleated cells did not differ significantly between the two muscle types (Fig. 5B), nor was a difference found in the fusion rate (Fig. 5C).

Gene expression profiling by DNA microarray analysis and qRT-PCR

Of approximately 21,000 genes analyzed using microarray, 7 showed higher expression in the SSP muscle than in the SSC muscle (Table 3). The levels of myosin-related

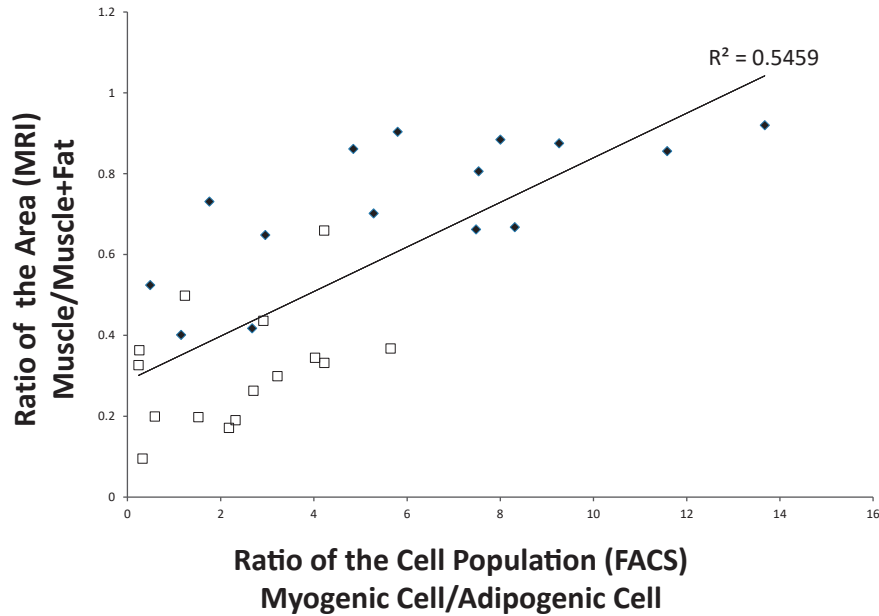


Fig. 2. Correlation between precursor ratio and magnetic resonance imaging (MRI) findings.

A positive correlation is observed between the ratio of myogenic precursors to adipogenic precursors and the ratio of the area of muscle tissue to total volume of muscle including fat tissue based on the MRI conducted before the surgery ($R^2 = 0.5459$, $P < 0.001$). Closed symbols indicate the values of SSC muscles and open symbols indicate the values of SSP muscles ($n = 15$ for each muscle).

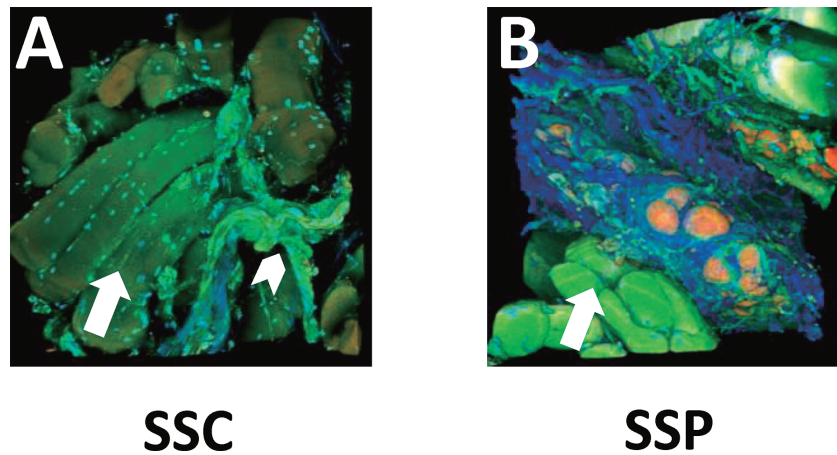


Fig. 3. Micro-structure of SSP and SSC muscle tissue samples evaluated using multi-photon three-dimensional imaging.

A: SSC muscle, B: SSP muscle. Muscle fibers exhibit green autofluorescence. Twisted blood vessels also appear green, but they are morphologically distinguishable from muscle fibers. The SSP muscle shows greater fatty infiltration surrounded by collagen fibers (blue) compared with the SSC muscle, as evidenced by BODIPY (red) staining (B). Arrows, muscle fibers; arrowhead, capillaries.

factors, such as myosin heavy chain (MYH) 2 and myosin light chain (MYL) 1 were higher in the SSP muscle, whereas seven showed higher expression in the SSC muscle than in the SSP muscle. The number of homeobox genes, such as homeobox (HOX) C4, HOX C6, HOXA11, and HOXA11-AS, was higher in the SSC muscles. The micro-array data have been deposited in the National Institutes of Health Gene Expression Omnibus (<https://www.ncbi.nlm.nih.gov/geo/query/acc.cgi?token=efijweowvlgpvap&acc=GSE93661>).

Seven genes showing higher expression in SSP and

another seven genes showing higher expression in SSC picked up by DNA microarray were evaluated using qRT-PCR. The upregulation of MYL1 in the disused muscle (SSPs) compared with in the intact muscle (SSCs) was confirmed. In contrast, the levels of voltage-gated potassium channel subfamily A member (KCNA)1 and of HOXA11 were downregulated in the SSP relative to the SSC (Table 4).

Discussion

The most important findings in this study were that

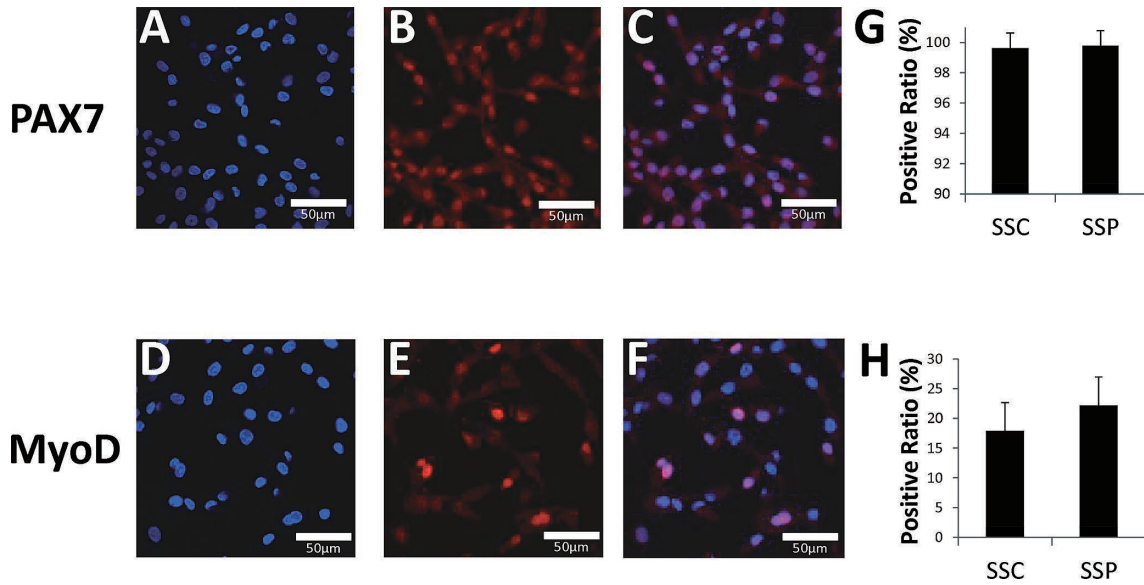


Fig. 4. Purity of satellite cells isolated using fluorescence-activated cell sorting (FACS). A-D: Immunofluorescence image of DAPI-stained nuclei (A and D) and PAX7 (B) and merged image of DAPI and PAX7 (C). E and F: Immunofluorescence image of myoblast determination protein (MyoD) without (E) or with (F) DAPI staining. Satellite cells isolated using FACS are labeled with antibodies against PAX7 or MyoD. G: Ratio of PAX7-positive cells in SSC and SSP. Most cells are PAX7 positive. H: Ratio of MyoD-positive cells in SSC and SSP. No statistical difference is found in the positive ratio in both groups.

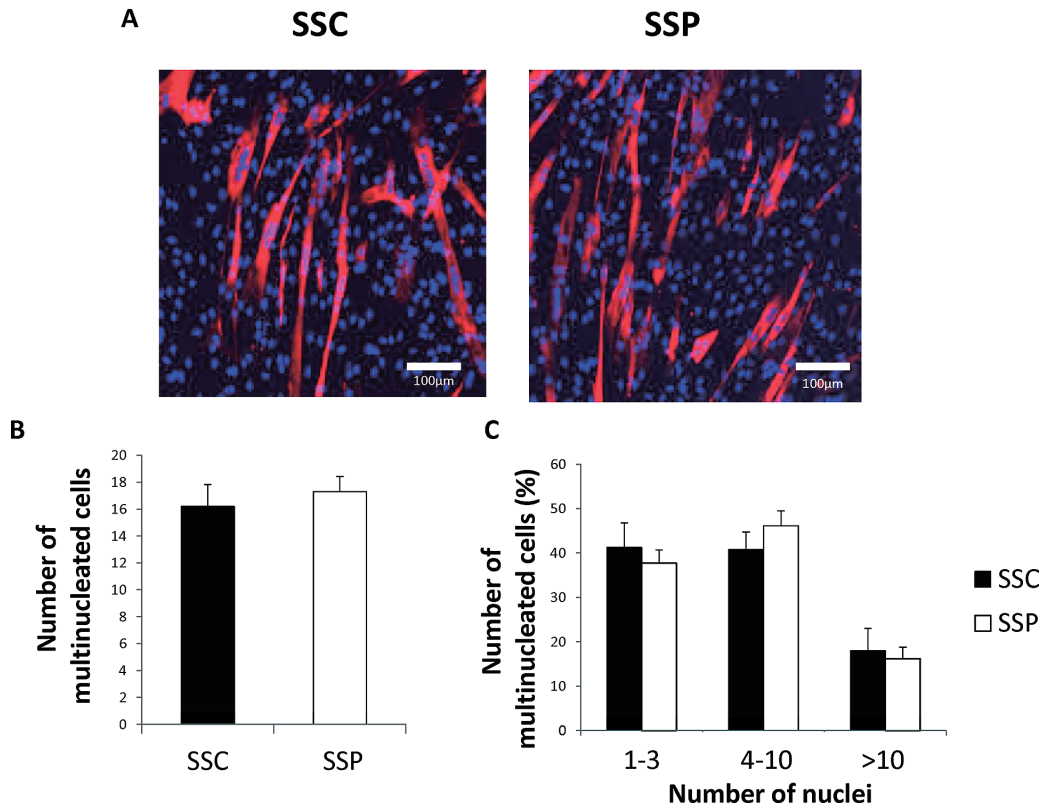


Fig. 5. Immunofluorescence analysis of myoblasts/myotubes. A: Immunofluorescence micrographs of myoblasts/myotubes labeled with anti-MHC antibody. B: Number of multinucleated cells in the SSC and SSP muscles. C: Fusion rate of SSC and SSP muscles. Immunofluorescence analysis of myoblasts/myotubes identified by myosin heavy chain (red) reveals satellite cells in both muscle types that are induced to differentiate into myoblasts/myotubes. No statistically significant difference was found between the SSP and SSC muscles in the number of multinucleated cells and fusion rate, determined by counting the number of nuclei (blue) in myotubes (DAPI, blue). Data represent mean \pm standard error of the mean.

Table 3. Gene expression profiling by DNA microarray.

GenBank	Gene Name	Description	Path1/Cont1 Fold change	Path2/Cont2 Fold change
NM_000041	ApoE	Apolipoprotein E, mRNA	2.354	1.915
NM_017534	MYH2	Myosin, heavy chain , skeletal muscle, adult, transcript variant 1, mRNA	2.926	1.731
NM_002422	MMP3	Matrix metalloproteinase 3 (stromelysin 1, progelatinase), mRNA	1.394	2.396
NM_005410	SEPP1	Selenoprotein P, plasma 1, transcript variant 1, mRNA	2.244	1.316
NM_079420	MYL1	Myosin, light chain 1, alkali: skeletal fast, transcript variant 1,mRNA	2.232	1.604
NM_000439	PCSK1	Proprotein convertase subtilisin/kexin type 1,transcript variant 1, mRNA	1.466	2.222
NM_031455	CCDC3	Coiled-coil domain containing 3, transcript variant 1, mRNA	1.051	2.197

GenBank	Gene Name	Description	Path1/Cont1 Fold change	Path2/Cont2 Fold change
NM_014620	HOX C4	Homeobox C4, transcript variant 1, mRNA	-3.502	-4.895
NM_004503	HOX C6	Homeobox C6, transcript variant 1, mRNA	-3.199	-3.621
NM_009586	SIM2	Single-minded family bHLH transcription factor, transcript variant SIM2s, mRNA	-1.527	-3.000
NM_000217	KCNA1	Potassium voltage-gated channel, shaker-related subfamily, member, mRNA	-1.133	-2.221
NM_005523	HOXA11	Homeobox A11, mRNA	-1.24	-2.189
NM_002795	HOXA11-AS	HOXA11 antisense RNA, antisense RNA	-1.664	-2.176
NM_004101	F2RL2	Coagulation factor II receptor-like 2, transcript variant 1,mRNA	-2.146	-1.333

Seven genes showed higher expression in the SSP muscle than in the SSC muscle (top), and seven genes showed higher expression in the SSC muscle than in the SSP muscle (bottom).

Table 4. Gene expression in the SSC and the SSP analyzed by qRT-PCR.

Gene	Muscle	Mean \pm SEM	<i>P Value</i>
ApoE	SSC	9.58 \pm 6.14	0.81
	SSP	5.57 \pm 3.53	
MYH2	SSC	6.12 \pm 3.51	0.35
	SSP	5.73 \pm 3.38	
MMP3	SSC	28.7 \pm 17.5	0.48
	SSP	1.46 \pm 0.75	
MYL1	SSC	22.5 \pm 13.0	<i>0.021</i>
	SSP	32.9 \pm 15.9	
SEPP1	SSC	1.94 \pm 1.31	0.17
	SSP	1.69 \pm 0.46	
PCSK1	SSC	30.9 \pm 29.1	0.88
	SSP	3.29 \pm 1.90	
CCDC3	SSC	19.6 \pm 11.1	0.46
	SSP	16.9 \pm 17.1	
HOX C4	SSC	15.3 \pm 10.3	0.42
	SSP	2.18 \pm 1.06	
HOX C6	SSC	41.4 \pm 20.0	0.15
	SSP	23.7 \pm 19.2	
SIM2	SSC	21.4 \pm 10.7	0.17
	SSP	7.66 \pm 4.56	
KCNA1	SSC	33.5 \pm 16.8	<i>0.033</i>
	SSP	5.12 \pm 2.98	
HOXA11	SSC	68.7 \pm 57.1	<i>0.010</i>
	SSP	22.5 \pm 18.0	
HOXA11-AS	SSC	2.58 \pm 1.89	0.86
	SSP	1.77 \pm 0.74	
F2RL2	SSC	24.4 \pm 15.5	0.13
	SSP	12.2 \pm 7.56	

Italic values significant at $P < 0.05$.

SSC, subscapularis; SSP, supraspinatus.

The upregulation of MYL1 in the SSP muscle compared with SSC muscle was confirmed. In contrast, the levels of KCNA1 and of HOXA11 were downregulated in the SSP relative to the SSC.

satellite cells from disused muscles (SSPs) with fatty infiltration could exhibit as much myogenic potential as those from intact muscles (SSCs), whereas the gene expression pattern of satellite cells showed significant differences between them.

The number of satellite cells in disused muscle is known to be reduced, caused by impaired proliferation (Zammit et al. 2006; Li et al. 2016). The mechanical stretch causes satellite cell activation (Imaoka et al. 2015). In this study, the satellite cells from disused muscle retained both their original proportions and myogenic potential as much as that from the intact muscle. These results suggest that satellite cells in disused muscles could be a therapeutic target for myogenic differentiation although the fatty infiltration of the muscle was severe. A previous study reported that a comparison of muscle precursors from bursitis and partial- and full-thickness RCT (Meyer et al. 2015) found no differences in muscle regeneration capacity, which was consistent with our results. In this study, arthroscopic surgery enabled us to accurately compare the nature of disused and intact muscles simultaneously in the same patients. Gigliotti et al. (2016) reported the denervation and potential for activation in disused muscle of RCT patients compared with the control group of the deltoid muscle. The reinnervation of disused muscle by mechanical stretching might be a therapeutic target for muscle growth in disused muscle.

The satellite cells in disused and intact muscles had equivalent myogenic potency, whereas their gene expression patterns showed significant differences. We collected paired muscle samples from each patient, which allowed us to perform highly accurate comparisons using paired statistical analysis. The DNA microarray and qRT-PCR analyses revealed increased myogenesis in satellite cells from disused muscle, as evidenced by MYH2 and MYL1 expressions. These genes are responsible for myosin structure and function (Laron et al. 2012). We also found that KCNA1 and HOXA11 levels were downregulated in disused muscle. HOXA11 negatively regulates the myogenic differentiation expression of the transcription factor myoblast determination protein in muscle precursors (Yamamoto et al. 2003), and KCNA1, a gene responsible for myokymia (Brownstein et al. 2016), suppresses myogenic contraction. These results suggest a myogenic shift of gene expression in satellite cells derived from disused muscle compared with the intact muscle. Thus, the satellite cells can be considered to compensate retained proliferation during the RCT with less physical load.

Our data showed that the number of adipogenic precursors increased in the disused muscle and was positively correlated with muscle atrophy severity, with a higher number in torn disused muscle than in the intact muscle. Although fatty infiltration and muscle atrophy are two main criteria for RCT severity (Laron et al. 2012; Fermont et al. 2014), the adipogenic precursor population in disused muscle has not been previously investigated. Although a small difference was observed in the population of adipogenic

precursors between disused and intact muscles, a significant difference was found in the adipogenic precursor/satellite cell ratio. Considering the fact that the satellite cells from disused muscles retained their original proportions, the increase of the adipogenic precursors would be explosive compared with the population of the satellite cells in disused muscles.

This study has some limitations. First, the SSC muscle was defined as the control, although it was derived from a pathological joint in the RCT and therefore did not have normal function. Second, although muscle atrophy was calculated from three series of Y-view images obtained using MRI, this may not accurately reflect muscle volume and fatty infiltration. Third, the increased or decreased expression of satellite cells may be in response to culture conditions of high serum and high CEE, matrigel, FGF-supplemented medium. Fourth, the number of sorted cells depended on the antibody markers, the specific region of the muscle that was biopsied, and the uniformity and extent of digestion by collagenase. Finally, we did not observe adipogenic precursor differentiation in culture, although the population size was correlated with muscle atrophy severity.

In conclusion, human satellite cells from the torn rotator-cuff SSP muscle with fatty infiltration maintained intrinsic myogenic potential and altered gene expression. Our results suggest that the satellite cells from the torn rotator-cuff SSP muscle can be used to develop therapeutic strategies that inhibit adipogenic precursor accumulation for effective RCT treatment.

Acknowledgments

This study was supported by Grant-in-Aid for Exploratory Research (Grant Number 16K15651).

Conflict of Interest

The authors declare no conflict of interest.

References

- Ariga, M., Nedachi, T., Katagiri, H. & Kanzaki, M. (2008) Functional role of sortilin in myogenesis and development of insulin-responsive glucose transport system in C2C12 myocytes. *J. Biol. Chem.*, **283**, 10208-10220.
- Asakura, A., Seale, P., Girgis-Gabardo, A. & Rudnicki, M.A. (2002) Myogenic specification of side population cells in skeletal muscle. *J. Cell Biol.*, **159**, 123-134.
- Bareja, A., Holt, J.A., Luo, G., Chang, C., Lin, J., Hinken, A.C., Freudenberg, J.M., Kraus, W.E., Evans, W.J. & Billin, A.N. (2014) Human and mouse skeletal muscle stem cells: convergent and divergent mechanisms of myogenesis. *PLoS One*, **9**, e90398.
- Barry, J.J., Lansdown, D.A., Cheung, S., Feeley, B.T. & Ma, C.B. (2013) The relationship between tear severity, fatty infiltration, and muscle atrophy in the supraspinatus. *J. Shoulder Elbow Surg.*, **22**, 18-25.
- Boldrin, L., Muntoni, F. & Morgan, J.E. (2010) Are human and mouse satellite cells really the same? *J. Histochem. Cytochem.*, **58**, 941-955.
- Brownstein, C.A., Beggs, A.H., Rodan, L., Shi, J., Towne, M.C., Pelletier, R., Cao, S., Rosenberg, P.A., Urion, D.K., Picker, J.,

- Tan, W.H. & Agrawal, P.B. (2016) Clinical heterogeneity associated with KCNA1 mutations include cataplexy and nonataxic presentations. *Neurogenetics*, **17**, 11-16.
- Davies, M.R., Liu, X., Lee, L., Laron, D., Ning, A.Y., Kim, H.T. & Feeley, B.T. (2016) Tgf- β small molecule inhibitor sb431542 reduces rotator cuff muscle fibrosis and fatty infiltration by promoting fibro/adipogenic progenitor apoptosis. *PLoS One*, **11**, e0155486.
- Fermont, A.J., Wolterbeek, N., Wessel, R.N., Baeyens, J.P. & de Bie, R.A. (2014) Prognostic factors for successful recovery after arthroscopic rotator cuff repair: a systematic literature review. *J. Orthop. Sports Phys. Ther.*, **44**, 153-163.
- Fuchs, B., Weishaupt, D., Zanetti, M., Hodler, J. & Gerber, C. (1999) Fatty degeneration of the muscles of the rotator cuff: assessment by computed tomography versus magnetic resonance imaging. *J. Shoulder Elbow Surg.*, **8**, 599-605.
- Gigliotti, D., Leiter, J.R., MacDonald, P.B., Peeler, J. & Anderson, J.E. (2016) Altered satellite cell responsiveness and denervation implicated in progression of rotator-cuff injury. *PLoS One*, **11**, e0162494.
- Gladstone, J.N., Bishop, J.Y., Lo, I.K. & Flatow, E.L. (2007) Fatty infiltration and atrophy of the rotator cuff do not improve after rotator cuff repair and correlate with poor functional outcome. *Am. J. Sports Med.*, **35**, 719-728.
- Goutallier, D., Postel, J.M., Bernageau, J., Lavau, L. & Voisin, M.C. (1994) Fatty muscle degeneration in cuff ruptures. Pre- and postoperative evaluation by CT scan. *Clin. Orthop. Relat. Res.*, **304**, 78-83.
- Hagiwara, Y., Ando, A., Onoda, Y., Takemura, T., Minowa, T., Hanagata, N., Tsuchiya, M., Watanabe, T., Chimoto, E., Suda, H., Takahashi, N., Sugaya, H., Saijo, Y. & Itoi, E. (2012) Coexistence of fibrotic and chondrogenic process in the capsule of idiopathic frozen shoulders. *Osteoarthritis Cartilage*, **20**, 241-249.
- Imaoka, Y., Kawai, M., Mori, F. & Miyata, H. (2015) Effect of eccentric contraction on satellite cell activation in human vastus lateralis muscle. *J. Physiol. Sci.*, **65**, 461-469.
- Judson, R.N., Zhang, R.H. & Rossi, F.M. (2013) Tissue-resident mesenchymal stem/progenitor cells in skeletal muscle: collaborators or saboteurs? *FEBS J.*, **280**, 4100-4108.
- Laron, D., Samagh, S.P., Liu, X., Kim, H.T. & Feeley, B.T. (2012) Muscle degeneration in rotator cuff tears. *J. Shoulder Elbow Surg.*, **21**, 164-174.
- Li, T.S., Shi, H., Wang, L. & Yan, C. (2016) Effect of bone marrow mesenchymal stem cells on satellite cell proliferation and apoptosis in immobilization-induced muscle atrophy in rats. *Med. Sci. Monit.*, **22**, 4651-4660.
- Liu, X., Ning, A.Y., Chang, N.C., Kim, H., Nissenson, R., Wang, L. & Feeley, B.T. (2016) Investigating the cellular origin of rotator cuff muscle fatty infiltration and fibrosis after injury. *Muscles Ligaments Tendons J.*, **6**, 6-15.
- Meyer, G.A., Farris, A.L., Sato, E., Gibbons, M., Lane, J.G., Ward, S.R. & Engler, A.J. (2015) Muscle progenitor cell regenerative capacity in the torn rotator cuff. *J. Orthop. Res.*, **33**, 421-429.
- Oh, J.H., Chung, S.W., Kim, S.H., Chung, J.Y. & Kim, J.Y. (2014) 2013 Neer Award: effect of the adipose-derived stem cell for the improvement of fatty degeneration and rotator cuff healing in rabbit model. *J. Shoulder Elbow Surg.*, **23**, 445-455.
- Perruchot, M.H., Lefaucheur, L., Barreau, C., Casteilla, L. & Louveau, I. (2013) Age-related changes in the features of porcine adult stem cells isolated from adipose tissue and skeletal muscle. *Am. J. Physiol. Cell Physiol.*, **305**, C728-738.
- Pfaffl, M.W. (2001) A new mathematical model for relative quantification in real-time RT-PCR. *Nucleic Acids Res.*, **29**, e45.
- Pisani, D.F., Clement, N., Loubat, A., Plaisant, M., Sacconi, S., Kurzenne, J.Y., Desnuelle, C., Dani, C. & Dechesne, C.A. (2010) Hierarchization of myogenic and adipogenic progenitors within human skeletal muscle. *Stem Cells*, **28**, 2182-2194.
- Tempelhof, S., Rupp, S. & Seil, R. (1999) Age-related prevalence of rotator cuff tears in asymptomatic shoulders. *J. Shoulder Elbow Surg.*, **8**, 296-299.
- Uezumi, A., Fukada, S., Yamamoto, N., Ikemoto-Uezumi, M., Nakatani, M., Morita, M., Yamaguchi, A., Yamada, H., Nishino, I., Hamada, Y. & Tsuchida, K. (2014) Identification and characterization of PDGFR α mesenchymal progenitors in human skeletal muscle. *Cell Death Dis.*, **5**, e1186.
- Uezumi, A., Fukada, S., Yamamoto, N., Takeda, S. & Tsuchida, K. (2010) Mesenchymal progenitors distinct from satellite cells contribute to ectopic fat cell formation in skeletal muscle. *Nat. Cell Biol.*, **12**, 143-152.
- Yabe, Y., Hagiwara, Y., Ando, A., Tsuchiya, M., Minowa, T., Takemura, T., Honda, M., Hatori, K., Sonofuchi, K., Kanazawa, K., Koide, M., Sekiguchi, T. & Itoi, E. (2015) Chondrogenic and fibrotic process in the ligamentum flavum of patients with lumbar spinal canal stenosis. *Spine (Phila Pa 1976)*, **40**, 429-435.
- Yamamoto, M. & Kuroiwa, A. (2003) Hoxa-11 and Hoxa-13 are involved in repression of MyoD during limb muscle development. *Dev. Growth Differ.*, **45**, 485-498.
- Yamayoshi, S., Fujii, K. & Koike, S. (2012) Scavenger receptor b2 as a receptor for hand, foot, and mouth disease and severe neurological diseases. *Front. Microbiol.*, **3**, 32.
- Zammit, P.S., Partridge, T.A. & Yablonka-Reuveni, Z. (2006) The skeletal muscle satellite cell: the stem cell that came in from the cold. *J. Histochem. Cytochem.*, **54**, 1177-1191.